Biophysical Journal
Article

Biophysical Society

Stochastic Subcellular Organization of Dense-Core Vesicles Revealed by Point Pattern Analysis

Benjamin J. Robinson,[1,2] Bogdan Stanisavljevic,[4] Michael A. Silverman,[4] and Bethe A. Scalettar[1,3,*]
[1]Department of Physics, [2]Department of Mathematics, and [3]Program in Biochemistry and Molecular Biology, Lewis & Clark College, Portland, Oregon; and [4]Department of Biological Sciences, Simon Fraser University, Burnaby, British Columbia, Canada

ABSTRACT Dense-core vesicles (DCVs) are regulated secretory organelles found in many types of neurons. In neurons of the hippocampus, their cargo includes proteins that mediate several pivotal processes, including differentiation and synaptic plasticity. Motivated by interest in DCV distribution and its impact on cargo action, we have used fluorescence microscopy and statistical analysis to develop a quantitative model of the subcellular organization of DCVs in hippocampal neurons that are spontaneously active (their most prevalent state). We also have tested the functionally motivated hypothesis that these organelles are synaptically enriched. Variance-to-mean ratio, frequency distribution, and Moran's autocorrelation analyses reveal that DCV distribution along shafts, and within synapses, follows Poisson statistics, establishing that stochastically dictated organization sustains cargo function. Occupancy in boutons exceeds that at nearby extrasynaptic axonal sites by approximately threefold, revealing significant local presynaptic enrichment. Widespread stochastic organization is consistent with the emerging functional importance of synaptically and extrasynaptically localized DCVs. Presynaptic enrichment is consistent with the established importance of protecting presynaptic sites from depletion of DCV cargo. These results enhance understanding of the link between DCV organization and mechanisms of cargo action, and they reinforce the emerging theme that randomness is a prevalent aspect of synaptic organization and composition.

INTRODUCTION

Cells use organelles to deliver cargo to, and localize cargo at, sites of function. Neurons, with their complex geometry and lengthy axons, must overcome significant challenges to ensure that these processes are implemented accurately and efficiently (1). How neurons accomplish this is a subject of intense interest because aberrations in organelle trafficking and targeting can lead to devastating medical conditions in the nervous system, including Alzheimer's disease (2).

Recently, substantial progress has been made in elucidating mechanisms underlying long-ranged transport of neuronal organelles between primary sites of synthesis in the soma and distal sites along axons and dendrites (3). One notable mechanism is rapid, motor-directed transport along microtubule-based tracks (4). Moreover, for some types of organelle (e.g., synaptic vesicles (SVs)), neurons reduce the required amount of long-ranged transport by recycling and reusing, and/or synthesizing, constituents more locally (e.g., at presynaptic sites) (5).

Mechanisms dictating the subcellular organization of neuronal organelles are somewhat less well understood (6). Typically, organelles are targeted to particular neuronal subdomains, and their distribution is thus highly nonuniform. In such cases, one common theme is that each unique, asymmetric distribution pattern is linked to a unique dynamic pattern generated by organelle-specific motors, adaptors, and scaffolding proteins (3).

In contrast, some neuronal organelles have a relatively broad subcellular distribution. In such cases, targeting can exist, but be subtle, or its existence still can be controversial. Mammalian dense-core vesicles (DCVs) (and mitochondria) are pertinent organelles of this type. DCVs are regulated secretory organelles found in many types of neurons in organisms spanning the spectrum from humans to *Drosophila*. In neurons of the hippocampus, DCVs house a diverse cargo, including molecules that mediate processes with wide-ranging spatial extent, such as growth (7). Consistent with such spatially broad cargo action, hippocampal DCVs frequently, but not universally (8,9), exhibit a visually broad and seemingly unpolarized subcellular distribution (10–12). In contrast, DCVs localize primarily to axons in organisms with less prominent dendrites, such as *Drosophila* and *Caenorhabditis elegans* (13–16).

Although DCVs in hippocampal neurons are broadly distributed, functional considerations nevertheless suggest plausible sites for their enrichment. One proposed site of

Submitted March 15, 2016, and accepted for publication July 5, 2016.
*Correspondence: bethe@lclark.edu
Editor: David Piston.
http://dx.doi.org/10.1016/j.bpj.2016.07.019

enrichment is the synapse because DCV cargo in hippocampal neurons includes proteins that play a pivotal role in synaptic plasticity (17–19). However, this hypothesis remains unproven. An alternative view is that DCVs localize, and undergo exocytosis, largely at extrasynaptic sites. Consistent with this competing view, DCV cargo in hippocampal neurons also mediates nonsynaptic functions, including survival, differentiation, and guidance (7). Moreover, local diffusion can lead to DCV cargo function at sites that are fairly distant (tens of microns) from sites of release (7,20).

Here we have experimentally tested the validity of the synaptic enrichment hypothesis, and determined the degree to which organization is stochastic, clustered, or uniform, for the case of DCVs in hippocampal neurons engaged in ongoing, spontaneous physiological activity, an established attribute of dissociated hippocampal cultures (21,22). Although once largely ignored, spontaneously active neuronal circuits are subjects of intense current interest because spontaneous activity is the most prevalent neuronal state and dominates total brain activity, and it is believed to play a critical role in the maturation of neural circuits (23–25). In our case, additional motivation stems from a relative paucity of past study of DCV organization in spontaneously active circuits and from evidence suggesting that spontaneous activity in hippocampal neurons induces release of the prominent DCV cargo protein brain-derived neurotrophic factor (BDNF) (26).

In past work, fluorescence microscopy has provided qualitative insight into DCV organization in many cell types, including hippocampal neurons (11,16,27,28). We instead have used fluorescence microscopy in conjunction with quadrat analysis and related statistical tools to study DCV organization quantitatively, facilitating detection and modeling of more subtle aspects of organization. Our data show that DCVs are distributed in a spatially uncorrelated pattern with the statistical properties of a Poisson process and that they localize with statistically indistinguishable occupancies to postsynaptic and extrasynaptic dendritic sites. In contrast, DCVs are locally enriched at presynaptic sites. We hypothesize that globally stochastic organization is biologically relevant for DCVs in hippocampal neurons because it sustains the wide-ranging actions of DCV cargo. Coexistent, small-scale presynaptic enrichment may protect presynaptic sites from DCV depletion (29,30). These results enhance understanding of the link between DCV organization and mechanisms of cargo action, and they reinforce the emerging theme that randomness is a prevalent aspect of synaptic composition (31).

MATERIALS AND METHODS

Cell culture

Hippocampal neurons were obtained from 18-day-old embryonic rats and cultured on No. 1.5 high-performance coverslips using standard techniques (32). Neurons were used when they were ~10 to ~21 days in vitro (DIV), depending on the experiment.

Construction and delivery of DNA

Expression vectors encoding fluorescent chimeras of DCV cargo proteins (e.g., the neuromodulatory proteins BDNF or tissue plasminogen activator, tPA) and enhanced green fluorescent protein, EGFP, or its spectral variants) were constructed using standard subcloning techniques (33). Vectors encoding fluorescent chimeras of synaptic markers or encoding soluble fluorescent-fill proteins were constructed similarly.

DNAs encoding fluorescent proteins were introduced into hippocampal neurons using transfection techniques based on viral infection, lipids, or electroporation (34,35). DNA was introduced into mature (>14 DIV) hippocampal neurons using a replication defective herpes simplex virus (35). Cells then were fixed or imaged 16–24 h after viral infection to avoid long-term expression of exogenous proteins. DNA was introduced into developing (~10 DIV) neurons using Lipofectamine 2000 (ThermoFisher Scientific, Waltham, MA), and cells were fixed or imaged 6–18 h after transfection. Finally, in a few cases, DNA encoding synaptic markers or fill proteins was introduced into freshly isolated hippocampal neurons via electroporation, following Amaxa's instructions for its Rat Nucleofector Kit (Lonza, Walkersville, MD).

Labeling of synapses, processes, and endogenous neuromodulators

Synaptic boutons and spines

We primarily used fluorescent chimeras to detect presynaptic axonal boutons, for reasons enumerated below. We also occasionally used immunostaining and obtained very similar results. To generate transfected samples expressing chimeras, we used either lipid-mediated delivery or electroporation to introduce DNA encoding a green or blue SV protein chimera, such as synaptophysin-EGFP. To generate immunostained samples, we used a primary rabbit polyclonal antibody against the endogenous presynaptic protein synapsin-1 (Synaptic Systems, Goettingen, Germany), following a protocol similar to that described in Lochner et al. (11). This primary antibody and others described below were detected with appropriate secondary antibodies.

We relied primarily on transfection and associated expression of exogenous soluble fluorescent proteins (e.g., enhanced blue fluorescent protein 2, EBFP2) to detect postsynaptic dendritic spines. Soluble proteins diffuse throughout (and fill) cells, which facilitates visualization of overall neuronal morphology and delineates spines (11).

In some cases, we explicitly confirmed that boutons and spines were synapsed (apposed) by labeling both domains. To this end, we used either a coculture approach or a double immunostaining approach. In the case of coculture, we labeled one set of neurons with synaptophysin-EGFP and another set with EBFP2. A 50:50 mix of the two cell types was then plated onto coverslips. This approach yielded coverslips on which fluorescent cells had labeled SV clusters or labeled spines, but not both. In the case of immunostaining, we labeled boutons as described above and spines using an affinity-purified antibody against postsynaptic density protein-95 (PSD-95; ThermoFisher Scientific). Such studies revealed 95% apposition (data not shown).

Axons and dendrites

To discriminate between axons and dendrites on more than morphological criteria, we immunostained hippocampal neurons using antibodies against the axonal-marker protein, tau-1 (36) (a gift from Dr. T. Frankfurter, University of Virginia, Charlottesville, VA), and the dendritic-marker protein, MAP-2 (37) (a gift from Dr. Shelley Halpain, Scripps Research Institute, San Diego, CA).

DCV cargo proteins

We also used transfection and immunostaining to label DCVs; however, we relied primarily on the former approach because it has several advantages. These include 1) the ability to study living cells; 2) low background, which greatly facilitates identification of DCVs; and 3) relative ease of complementary double-immunostaining to facilitate definitive identification of both axons and dendrites. The primary disadvantage of transfection is the possibility of overexpression-induced artifacts. However, a body of work suggests that overexpression in our system is quite modest and that associated artifacts are not a problem (12,19,38,39). Nevertheless, as a control, we also analyzed samples consisting of endogenous DCV cargo tagged with antibodies.

For our control work, we immunostained the endogenous DCV proteins BDNF or tPA. In the case of BDNF, we used a sheep anti-BDNF antibody (Millipore, Billerica, MA) that has been used previously to detect endogenous BDNF in hippocampal neurons (19,40). In the case of tPA, we affinity-purified a goat anti-tPA antibody (Millipore), as described in Lochner et al. (19).

Imaging

Sample preparation

In preparation for fixed imaging, neurons attached to coverslips were fixed for 15 min in 4% paraformaldehyde/4% sucrose in phosphate-buffered saline (PBS, pH 7.4) warmed to 37° C. After fixation, coverslips were rinsed three times with PBS and then were mounted in elvanol or Prolong Antifade (ThermoFisher) and sealed to a slide with clear nail polish.

In the case of live imaging, coverslips containing hippocampal neurons were mounted in a chamber in Hanks-based imaging medium augmented with 10 mM HEPES and 0.6% glucose. The chamber was maintained at ~35°C.

Approaches

High-resolution, multicolor images of fixed neurons were generated using two wide-field fluorescence microscopy systems. In most cases, three-dimensional images were collected by optically sectioning cells in 0.2 μm focal increments using a DeltaVision wide-field optical sectioning microscopy system (GE Healthcare Life Sciences, Issaquah, WA). These images were computationally deblurred using a constrained iterative deconvolution algorithm to improve clarity, as described in Scalettar et al. (41). In a few cases, images of fixed neurons were generated instead on an Axiovert Observer Z1 microscope (Carl Zeiss Microscopy, Thornwood, NY).

Several fluorescence microscopy systems were used for time-lapse imaging of living neurons, most commonly the Axiovert (Carl Zeiss Microscopy). Time-lapse images of DCV transport in living cells were generated by taking images of the same focal plane every several hundred milliseconds.

Image analysis and data quantification

Identification of boutons and spines

Morphological, staining, and mobility criteria were used to choose spines and boutons for analysis. Morphological criteria largely sufficed for spines, which are readily identifiable in both fixed and living samples as projections from the dendritic shaft consisting of a shaft and head. Nevertheless, postsynaptic proteins, such as PSD-95, also sometimes were tagged to aid in identifying spines. Morphological criteria were less satisfactory for boutons, because boutons and transport vesicles containing SV precursors have a somewhat similar appearance, and both line the axon shaft. Thus, in the vast majority of cases, we also invoked an immobility criterion, similar to past work (42). Specifically, we collected movies, and we restricted our choice of boutons to larger immobile, bright fluorescent puncta. In all cases, to avoid bias, spines and boutons were identified, and chosen for analysis, by examining only the color channel in which these structures appeared.

Identification of effectively immobile DCVs

In some cases, we wanted to map the distribution of just the immobile DCV pool. To this end, DCVs were defined as effectively immobile if their displacement in a movie (spanning minutes) was less than or equal to the associated root-mean-squared displacement of an organelle undergoing extremely slow diffusion in two dimensions, consistent with past work (43,44). The relevant root-mean-squared displacement, $\langle r^2\rangle^{1/2}$, in μm was computed using the diffusion expression (45,46):

$$\langle r^2\rangle^{1/2} = (4Dt)^{1/2},$$

where the diffusion coefficient, D, was assigned the very small value, $D = 5 \times 10^{-12}$ cm^2/s $= 5 \times 10^{-4}$ μm^2/s. A typical time, t, for our movies was t ~120 s, and thus a typical upper-bound on displacement was $\langle r^2\rangle^{1/2} = [4(5 \times 10^{-4})120]^{1/2} = 0.5$ μm. DCVs that underwent a displacement smaller than this value during the course of a movie were defined as effectively immobile.

Validation of area-based approaches

Quadrat and enrichment analyses (see below) can be implemented by quantifying (DCV fluorescence)/area or (DCV fluorescence)/volume, and it is not obvious which of these two approaches has greater biological significance. We adopted an area-based approach, which is technically more straightforward, for three reasons. First, in most cases, use of area or volume does not alter conclusions. This is true because structures like extrasynaptic regions of an axonal shaft have a relatively constant thickness and are relatively thin. Thus, fluorescence signals include out-of-focus pickup from the entire depth/volume for our wide-field systems (47). This in turn implies that total fluorescence intensity from all observed parts of the specimen is contained in a single optical section and that fluorescence per area and per volume differ only by an overall factor of thickness, which is irrelevant for comparative purposes. The second and third reasons to favor an area-based approach are that 1) our axonal data were obtained from time-lapse movies of a single focal plane, and 2) we want to compare our data with relevant mitochondrial data, which were determined using area-based approaches (42,48).

There are two important cases, which arise in our analysis of enrichment, where assuming an approximately constant structural thickness is potentially problematic. The most obvious of these is when we compare signal from boutons (putative axonal swellings) to those from extrasynaptic axonal sites (49). The other (analogous) case is when we compare signals from spines to those from extrasynaptic dendritic sites. For these cases, we quantified possible thickness differences by comparing integrated fluorescence signals generated by a soluble fill, using areas superimposed on synapses and areas superimposed on analogously sized extrasynaptic sites. Samples used for these studies were either cotransfected with green- or blue-tagged SVs and with a spectrally compatible blue or green protein fill (bouton/axon case) or with just a blue fill (spine/dendrite case).

Statistical methods

Point pattern analysis comprises a set of approaches that are designed to find patterns in spatial distributions of objects that can be approximated as points (50). Among these approaches, quadrat analysis is intuitive, reliable, and simple to implement. Thus, it is one of the main approaches adopted here.

Quadrat analysis

To implement quadrat analysis, we followed standard protocols and separated the region of interest (ROI; e.g., part of an axon) into boxes/quadrats and counted the number of DCVs (objects) per quadrat manually, as shown schematically in Fig. 1 *A*. To choose an appropriate quadrat area,

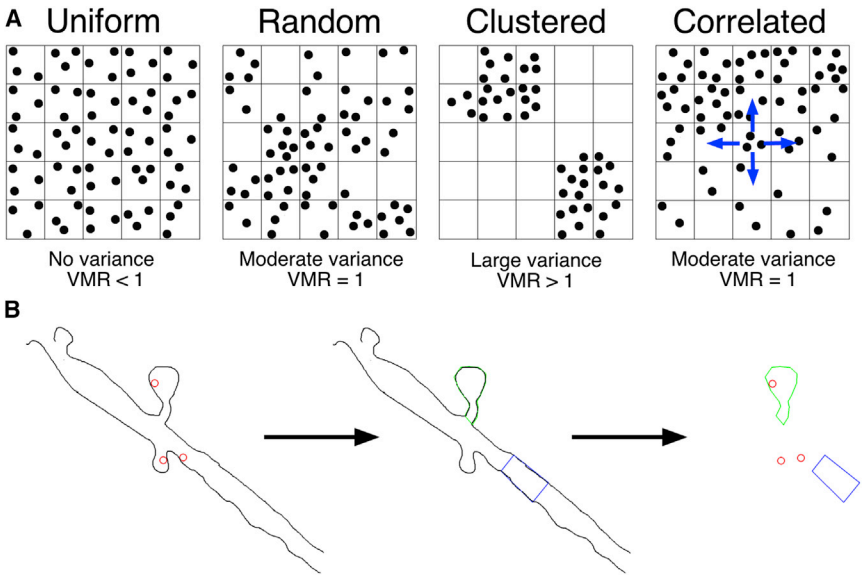

FIGURE 1 Schematized implementation of (*A*) VMR and (*B*) FO analyses. The 25 quadrats in the "Correlated" panel are a spatially correlated rearrangement of the 25 quadrats in the "Random" panel. Superimposed on the "Correlated" panel are arrows that show rooks neighbors for the middle quadrat. The lower-left sketch shows DCVs (*red*) along a dendrite outlined in gray. The lower-middle sketch shows quadrats of equal area superimposed on the dendrite; one is drawn around a spine (*green*) and the other is drawn around an extrasynaptic site (*blue*). The lower-right sketch shows the quadrat image superimposed on the image of the DCVs to facilitate computation of FO values. To see this figure in color, go online.

A_{quadrat}, we followed the standard rule-of-thumb, which is meant to avoid problems associated with a choice of quadrat size that is either too small or too large. It suggests that an ideal quadrat area should lie approximately in the range (51):

$$A_{\text{quadrat}} = \left(\frac{A_{\text{ROI}}}{N}, \frac{2 \times A_{\text{ROI}}}{N}\right).$$

In this expression, A_{ROI} is the area of the entire ROI, and N is the total number of objects in the ROI. Although this rule-of-thumb is well accepted, we checked, when possible, for consistency of results using several different quadrat sizes to rule out artifacts related to choice of sampling scale. We also verified that use of average synaptic area, as described for a few cases below, is approximately consistent with this rule.

Variance-to-mean ratio test

We quantified quadrat count data using three approaches. In the first approach, data were entered into Excel (Microsoft, Redmond, WA) and used to compute the mean number of objects per quadrat, the associated variance, and their ratio, the variance-to-mean ratio (VMR).

The utility of the VMR stems from its ability to distinguish uniform (repelling), stochastic/random (Poisson), and clustered (attracting) distributions based on their progressively increasing VMRs (48,52). When distribution is uniform, the variance is low (ideally zero), and the $VMR < 1$. When distribution is stochastic/random (i.e., described by the Poisson distribution), the mean and variance are equal, and the $VMR = 1$. Finally, when distribution is clustered, the variance is larger than the mean, and the $VMR > 1$.

Frequency distribution analysis

In the second approach, experimentally observed frequencies in quadrats (i.e., probabilities) were compared with theoretically predicted frequencies derived from relevant distribution functions. Although more involved, frequency distribution analysis (FDA) is in some respects an improvement over VMR analysis because it uses more than a single parameter to describe distribution in the ROI.

To implement FDA, we compared experimental point patterns to Poisson, Gaussian, and uniform/single-valued patterns. These were described, respectively, by the density functions (53):

$$P_P\,(m,\mu) = \frac{\mu^m}{m!}e^{-\mu},$$

$$P_G\,(m) = \frac{1}{\sigma\sqrt{2\pi}}e^{-\frac{1}{2}\left(\frac{m-\mu}{\sigma}\right)^2},$$

$$P_U = \delta\,(m-\mu).$$

In the equations above, $P_P(m,\mu)$ describes the Poisson probability of finding an integral number of objects m in an area, given that the mean number of objects/area is μ; P_G similarly describes the Gaussian probability of finding m (not necessarily integral) objects, given that the mean and standard deviation are, respectively, μ and σ; and P_U describes the uniform, single-valued, δ-function probability of finding the average number of objects in each quadrat.

Moran's I autocorrelation analysis

In the third approach, we implemented a spatial autocorrelation test to confirm or refute the idea that quadrat counts at one location are independent of counts in a neighboring location. This test was implemented to overcome a limitation of VMR and similar analyses, which is insensitivity to potential nonrandomness that arises from clustering of quadrats with similar (or dissimilar) counts (see Fig. 1 *A*).

One well-established quantitative test for the existence of spatial autocorrelation in discrete and continuous data values, X_i, measured over M regions/quadrats is Moran's I, which is structurally similar to Pearson's correlation coefficient and is defined as (51,54–56):

$$I = \frac{M}{\sum_{i=1}^{M}\sum_{j=1}^{M}w_{ij}}\frac{\sum_{i=1}^{M}\sum_{j=1}^{M}w_{ij}\left(X_i-\overline{X}\right)\left(X_j-\overline{X}\right)}{\sum_{i=1}^{M}\left(X_i-\overline{X}\right)^2},$$

$$I = [+1,-1],$$

where $\overline{X}$ is the data mean, and the w_{ij} values are spatial weights (see below). The definition of Moran's I ensures that positively correlated neighboring values, which similarly differ in being above or below the mean, contribute positively to I, whereas negatively correlated values contributed negatively to I. For a random spatial distribution, positive and negatives sum to zero and $I = 0$, as long as M is relatively large. Moreover, Moran's I is normalized so that $I = \pm 1$ under conditions of maximal positive/negative correlation, except in unusual cases.

Implementation of the Moran's I test requires choosing how to weight neighbor relations. We followed the most common procedure and set $w_{ij} = 1$ when quadrats are contiguous consistent with straight line, chess-based "rooks" moves (depicted using arrows in the rightmost panel in Fig. 1 *A*), and $w_{ij} = 0$ otherwise. In a few cases, we implemented another similar, standard weighting and set $w_{ij} = 1$ consistent with "queens" moves and $w_{ij} = 0$ otherwise, and verified consistency of results.

Area-based assays for synaptic enrichment

To facilitate comparison with other germane studies, and because quadrat analysis has some limitations, we also assayed for synaptic enrichment using fractions occupied (FO) and mean fluorescence intensities, $\langle F \rangle$; see Fig. 1 *B*. FO values were measured for "quadrats" positioned on synaptic sites and on analogous, nearby, extrasynaptic sites and were computed for each type of site (e.g., bouton, spine, extrasynaptic shaft site) using the expression:

$$FO_{\text{type of site}} = \frac{\left(\begin{array}{c}\text{number of quadrats}\\ \text{occupied by at least one DCV}\end{array}\right)}{(\text{total number of quadrats})},$$

similar to past work (42).

The FO is a measure of "yes" or "no" on occupancy and fails to take into account effects of having multiple DCVs in a quadrat. Thus, we also assayed for enrichment using mean fluorescence intensities, $\langle F \rangle$, from synaptic sites and nearby subdomains of shafts. To calculate $\langle F \rangle$, we used the ROI Manager tool in Fiji/ImageJ (National Institutes of Health, Bethesda, MD) to tabulate total synaptic signals and areas. These data were entered into Excel, separately summed, and $\langle F \rangle$ was computed from their ratio. A similar procedure was implemented for extrasynaptic sites, where the area of these sites was set equal to the average synaptic area.

Statistical significance of data

Data are reported as $\mu \pm \sigma$, where μ and σ were computed from data pooled from n different cells and/or cell cultures where, in all cases, $n \geq 3$. Statistical similarities and differences between data means were analyzed using the two-tailed Student's t-test function in the software Excel and are reported in terms of p values. For the t-test analysis, we adopted the standard 95% confidence criterion and assumed that two data sets were statistically different if $p < 0.05$ and were statistically similar if $p > 0.05$.

Similarity between experimental data and data derived from theoretical distributions was assessed using the chi-squared, χ^2, goodness-of-fit test statistic, which is defined as (57):

$$\chi^2\,(df) = \sum_{i=1}^{k} (O_i - E_i)^2 / E_i,$$

where O_i and E_i are, respectively, the experimentally observed and theoretically expected counts of i DCVs per quadrat, and the independent variable, df = k−2, is the number of degrees of freedom when the test is applied to the Poisson distribution. The χ^2 test was adopted because of its wide domain of validity, particularly its applicability to both continuous and discrete distributions, as studied here. For the χ^2 analysis, we again assumed that, if $p > 0.05$, there is too little difference between the experimental data and data derived from a comparative distribution to justify a conclusion that they differ.

Statistical significance of the deviation of an individual value of I from the value of I expected for a random distribution (essentially zero) can be assessed using a p value (z-score) formula derived from a random permutation procedure (58). The formula is very complicated, but in cases of larger disparity from zero (e.g., $I = 0.137$), we calculated p values to assess if the I value suggested a statistically significant (albeit small) degree of spatial autocorrelation.

RESULTS

Microscopy has helped to establish that many classes of organelle are substantially (e.g., visibly) enriched at spatially restricted subcellular domains that correspond to sites of intense cargo function and/or release. In contrast, microscopy-based studies of DCVs in mammalian neurons typically do not provide qualitatively obvious evidence for enrichment; thus, this putative effect is at most subtle and must be assayed using quantitative, statistical methods (11,19,59), such as those shown schematically in Fig. 1. Statistical methods also are needed to assess the degree of randomness in DCV organization. Motivated by importance and lack of relevant data, we have focused on DCV organization in neurons engaging in ongoing, spontaneous activity, which is an established property of dissociated hippocampal cultures (22).

VMR analysis supports the hypothesis that DCVs are organized randomly along processes

We implemented the VMR test using neurons expressing fluorescent chimeras of DCV cargo, and using neurons that were immunostained against endogenous DCV cargo proteins, and checked the results for consistency.

Fig. 2 *A* shows representative images of subregions of transfected hippocampal neurons expressing the chimeric cargo protein tPA-EGFP that also were immunostained to distinguish axons from dendrites. In these images, there is no visually obvious inhomogeneity in DCV distribution along processes, consistent with past work suggesting an absence of site-specific enrichment that is evident from qualitative analysis (11,19,60).

To prepare the image in Fig. 2 *A* for quantitative analysis, processes were divided into quadrats and DCVs were

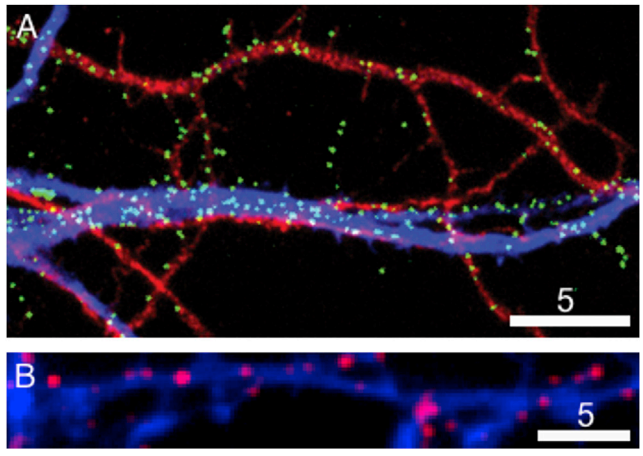

FIGURE 2 Subregions (*A*) of 16 DIV hippocampal neurons expressing tPA-EGFP (*green*) that also were immunostained to distinguish axons (*red*) from dendrites (*blue*) and (*B*) of a 17 DIV hippocampal neuron expressing a soluble fill (*blue*) that also was immunostained to visualize endogenous BDNF (*red*). Scale bars = 5 μm. To see this figure in color, go online.

approximated as points. Quantification of the resulting quadrat-count data from this, and other, fixed transfected hippocampal neurons gave an axonal $VMR = 0.94 \pm 0.15$ ($n = 429$ DCVs) and a dendritic $VMR = 1.29 \pm 0.43$ ($n = 721$ DCVs). Notably, point objects with a Poisson distribution give rise to a $VMR = 1$; thus, these data suggest that chimerically tagged DCVs in spontaneously active neurons are distributed essentially randomly over large-scale regions of processes.

Fig. 2 *B* similarly shows a representative image of a subregion of a neuron immunostained against the endogenous DCV cargo protein BDNF. These and other images of immunostained neurons also were subjected to the VMR test, and quantification of the resulting data gave an axonal $VMR = 0.85 \pm 0.07$ ($n = 232$ DCVs) and a dendritic $VMR = 0.85 \pm 0.23$ ($n = 227$ DCVs). These results for endogenously tagged DCVs are slightly lower than, but statistically indistinguishable from, results obtained for chimerically tagged DCVs ($p = 0.29$ (axon) and $p = 0.11$ (dendrites)), and they again suggest that distribution over processes is predominantly stochastic. A possible reason that immunostained samples yield VMRs that are slightly more suggestive of uniformity is that they possess a higher background.

The images in Fig. 2, and their associated VMR data, reflect the distribution of mobile and immobile DCVs, consistent with past VMR analysis of mitochondrial organization in neurons (48). However, the immobile DCV fraction, which can be identified using living samples, has unique, putative functional importance (44,61,62). We thus did a separate VMR analysis of immobile DCVs along axons, using the movies that we collected to study DCV localization at boutons and the definition of effective immobility described under Materials and Methods.

Fig. 3 shows a representative image used to implement this analysis. Putative immobile DCVs were first identified as puncta that appeared yellow in images generated by overlaying the first (encoded *green*) and last (encoded *red*) time point of the DCV channel in a movie. Immobility then was confirmed by scrolling through the associated movie to eliminate fortuitous overlap of two distinct DCVs that produced yellow and to identify immobile DCVs that did not appear yellow because they underwent a slight displacement during the movie. Implementing such an analysis on this, and similar images, yielded an axonal $VMR = 1.04 \pm 0.35$ ($n = 108$ DCVs). This result also suggests random organization of just the immobile fraction.

Spatial correlation analysis solidifies the evidence for randomness

Although consistent with spatial randomness, the quadrat-based VMR results presented above leave open the possibility of spatial correlations in DCV positions, which would be indicative of nonrandomness, as shown in Fig. 1 *A*. To address this possibility, we implemented Moran's *I* test, which is a well-established tool for spatial autocorrelation analysis in the fields of geography and ecology and recently has been used to quantify correlations in protein distribution at the *Drosophila* neuromuscular junction (63).

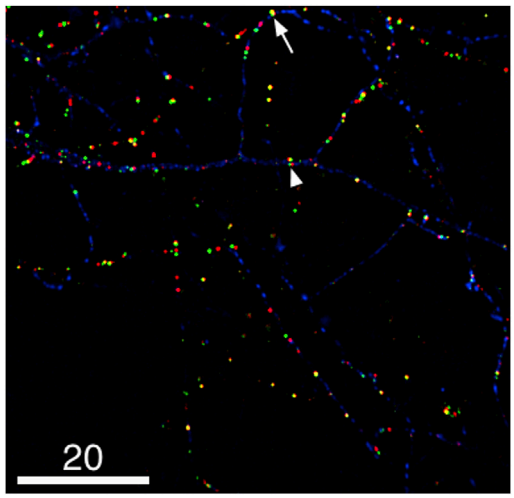

FIGURE 3 Subregions of 17 DIV hippocampal neurons expressing BDNF-mCherry and synaptophysin-EGFP. In this image, green reveals DCV positions at an initial time point, red reveals DCV positions at a final time point (~2 min later), and blue reveals the distribution of synaptophysin-EGFP (putative axonal boutons). Completely immobile DCVs appear yellow due to overlapping green and red puncta (*arrow*). Effectively immobile DCVs appear as closely apposed green and red puncta due to a slight displacement (e.g., ~0.3 μm) during the course of the movie (*arrowhead*). Scale bar = 20 μm. To see this figure in color, go online.

Moran's *I* was computed for axonal and dendritic structures using images such as those shown in Fig. 2. The visual impression from the images is an absence of any marked spatial correlation in DCV positions. More quantitatively, we found $I = 0.073 \pm 0.048$ ($n = 144$ quadrats) and $I = 0.001 \pm 0.114$ ($n = 160$ quadrats) for axonal and dendritic structures, respectively. Both of these average results are extremely close to the value, $I = 0$, that is expected for a random spatial distribution. Moreover, individual values of *I* did not differ in a statistically significant way from zero ($p >> 0.05$). Thus, spatial correlation analysis strongly reinforces the conclusion that DCVs are organized randomly along processes.

FO and $\langle F \rangle$ reveal presynaptic enrichment of DCVs

To enhance reliability, we used two approaches to assay for enrichment of DCVs in pre- and postsynaptic sites relative to nearby regions along shafts. These were computation of FO values and mean fluorescence intensities, $\langle F \rangle$; computation of FO values also facilitated comparison with related work on mitochondria (see Discussion).

For our presynaptic work, we primarily studied living samples to facilitate identification of SV protein chimera-tagged

structures that were immobile. Specifically, larger immobile structures were taken to represent boutons instead of transport packets for SV precursors, consistent with past work (42). In contrast, in our postsynaptic work, we studied both fixed and living samples because spines are more straightforward to identify without invoking an immobility criterion.

Fig. 4 *A* shows a representative example of images that were used to measure and compare FO values. Quantification of images of neurons labeled with chimerically tagged cargo revealed that $FO_{\text{bouton}} = 0.51 \pm 0.12$ ($n = 164$ sites) and $FO_{\text{axonshaft}} = 0.23 \pm 0.11$ ($n = 110$ sites), and that these two types of *FO* are statistically distinguishable ($p = 0.03$). Quantification of analogous dendritic data revealed that $FO_{\text{spine}} = 0.41 \pm 0.11$ and $FO_{\text{dendriticshaft}} = 0.42 \pm 0.17$ (in both cases, $n = 131$ sites), and that these results are statistically indistinguishable ($p = 0.93$). These data suggest that axonal DCVs are presynaptically enriched in spontaneously active hippocampal neurons, but they refute synaptic enrichment for the case of dendritic DCVs.

To generate a simple quantitative measure that summarizes enhancement effects, we computed an enhancement ratio (ER) for boutons and spines as the ratio of occupancy in each type of synaptic site to occupancy in the analogous extrasynaptic site, e.g., $ER_{\text{bouton}} = FO_{\text{bouton}}/FO_{\text{axonshaft}}$. We found $ER_{\text{bouton}} = 2.55 \pm 0.84$ and $ER_{\text{spine}} = 1.09 \pm 0.54$.

One potential limitation of an FO value is its failure to distinguish sites that contain one DCV from those that contain larger number of DCVs. Thus, FO values will not detect bias that arises from accumulation of multiple DCVs in occupied sites. To address this limitation, we computed $\langle F \rangle$ in the DCV channel for synaptic and for associated extrasynaptic sites and its associated *ER*, which is independent of variable raw fluorescence intensities. The results so obtained, $ER_{\text{bouton}} = 3.26 \pm 1.15$ ($n = 127$ sites) and $ER_{\text{spine}} = 0.70 \pm 0.44$ ($n = 111$ sites), were indistinguishable from the analogous *FO* results ($p = 0.33$ and 0.27, respectively).

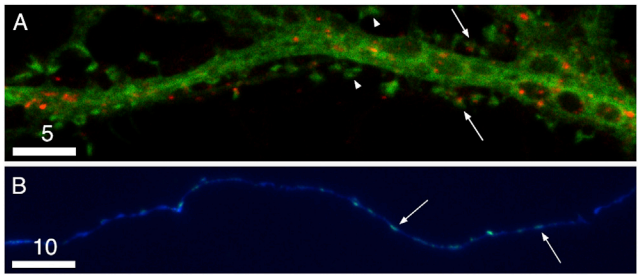

FIGURE 4 Subregion (*A*) of a 21 DIV hippocampal neuron that was used to quantify putative postsynaptic enrichment of DCVs in dendritic spines. This neuron is expressing a soluble fill protein (*green*) and tPA-mCherry (*red*). Two spines containing DCVs are identified with arrows and two devoid of DCVs are identified with arrowheads. Subregion (*B*) of a 10 DIV hippocampal neuron that was used to quantify relative thicknesses of boutons and extrasynaptic axonal sites. This cell was expressing a soluble fill protein (*blue*) and synaptophysin-EGFP (*green*). Two boutons are identified with arrows. Scale bars = 5 and 10 μm. To see this figure in color, go online.

To quantify possible disparities between area- and volume-based enrichment analyses, we measured integrated fluorescence (IF) signals generated by a soluble fill and compared values from areas centered on boutons or spines to those from similarly sized areas centered on extrasynaptic axonal sites. This approach allowed comparison of the effective thicknesses of shafts and synapses, where the term "effective" is used because organelles, like SVs, might significantly reduce the total volume accessible to the fill and to DCVs. If effective thicknesses are similar, disparities are likely to be minimal.

Fig. 4 *B* shows a representative image that was used to measure IFs and the signal ratio $IF_{\text{bouton}}/IF_{\text{axonshaft}}$. Quantification of data from this and similar images revealed that $IF_{\text{bouton}}/IF_{\text{axonshaft}} = 0.93 \pm 0.27$ ($n = 50$ sites), indicating that effective thicknesses of boutons and extrasynaptic axonal sites are very similar in our cells. An analogous procedure applied to spines revealed that $IF_{\text{spine}}/IF_{\text{dendriteshaft}} = 0.69 \pm 0.10$ ($n = 50$ sites), suggesting, in contrast, that spines are somewhat thinner than dendritic shafts in our cells. However, the effect is not large enough to alter the conclusion that enhancement in spines as a function of volume is at most a relatively minor effect.

FDA demonstrates that DCV occupancy of synapses is a Poisson process

FDA is a powerful, but more involved, method of determining the statistical properties of organization. Given its power, we used FDA as a final method of quantifying organization. Our major application was to synapses because these are especially pivotal sites.

To implement FDA, we measured the mean number of DCVs/synaptic site, μ; the associated standard deviation, σ; and the probabilities that a synaptic site contains m DCVs, where $m = 0, 1, 2, 3$, etc. We then compared the data with Poisson, Gaussian, and uniform distributions as defined under Materials and Methods. These were constructed using the experimentally measured μ and σ.

Fig. 5 *A* shows a plot of our experimental data for the case of spines for $m = 0, 1, 2, 3, 4$ ($n = 199$ spines/138 DCVs). Also shown are plots of data derived from the three comparative patterns using $\mu = 0.69$ and $\sigma = 0.81$, which were determined experimentally. The agreement between experiment and the Poisson distribution is visually excellent, but with the other distributions is poor. Moreover, implementation of the χ^2 goodness-of-fit test yielded $\chi^2 = 1.47$ and $p = 0.69 >> 0.05$, which quantitatively confirmed an excellent fit to the Poisson distribution.

Fig. 5 *B* similarly shows a plot of our experimental data for boutons ($n = 182$ boutons/141 DCVs) together with plots of comparative theoretical patterns obtained with

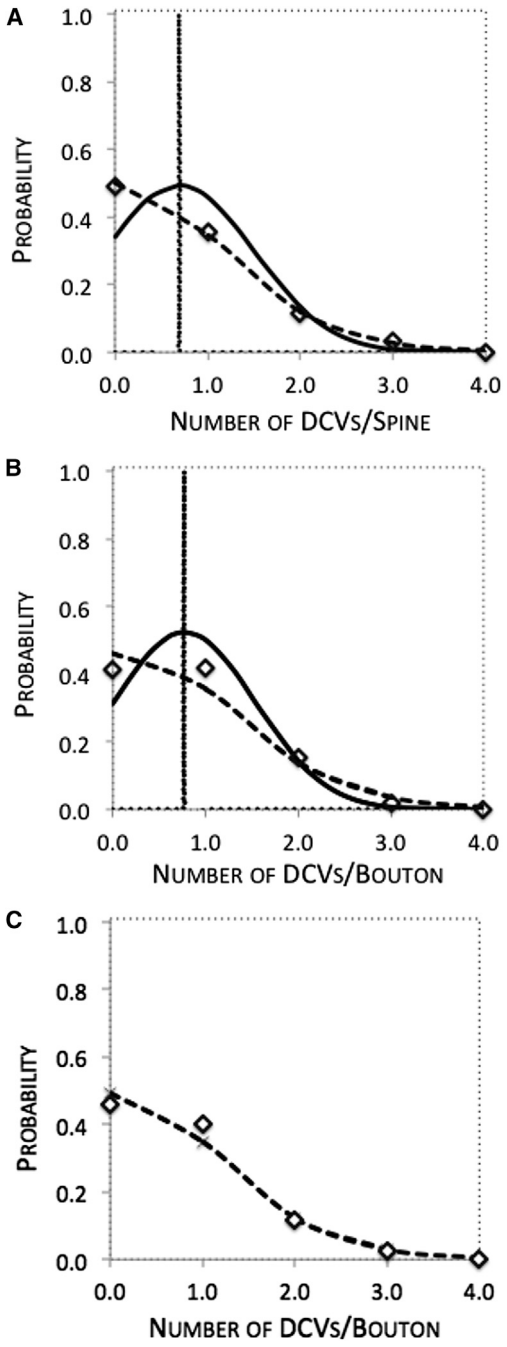

FIGURE 5 Plots of occupancy probabilities for (*A*) spines and (*B* and *C*) boutons versus DCV occupancy number deduced from experimental measurement (*diamonds*) and from the Poisson (*dashed line*), Gaussian (*solid line*), and uniform (*dotted line*) distributions, where μ and σ in the theoretical distributions were assigned their experimental values. The experimental plots in (*B*) and (*C*) differ slightly because only immobile DCVs contribute to the data in (*C*).

associated experimental parameters ($\mu = 0.77$ and $\sigma = 0.76$). The experimental data again appear visually to be quite well fit by the predictions of the Poisson distribution, although there is a little more disparity than in the case of spines. In particular, the observed probabilities are somewhat higher than the corresponding Poisson predictions for the cases of one and two DCVs per bouton. The observed probability also is somewhat lower than the Poisson prediction for the case of zero DCVs per bouton. Consistent with these small disparities, implementation of the goodness-of-fit test yielded $\chi^2 = 6.27$ and $p = 0.10$, indicating that the fit to a Poisson distribution is reasonable but not nearly as flawless as for the case of spines. A more compelling fit is obtained when only immobile DCVs are included, as described next.

Because we studied living samples, we also were able to apply FDA just to immobile DCVs, which are long-lived residents of boutons. As mentioned above, this pool has unique, putative functional importance, and its separate analysis, using living samples, is of interest because many DCVs that overlap with fixed boutons simply were passing transiently through the bouton at the time of fixation. This is not true for DCVs that overlap with fixed spines because DCVs that enter spines are trapped for long times (11).

Fig. 5 *C* shows a plot of our experimental results on the distribution of immobile DCVs in boutons ($n = 120$ boutons/85 DCVs) together with a plot of just the comparative Poisson pattern ($\mu = 0.71$). The overall message is a similar, but more compelling, argument for randomness. Specifically, visual analysis and the goodness-of-fit test, which yielded $\chi^2 = 1.92$ and $p = 0.59$, both support a Poisson model of organization.

DISCUSSION

Organelles often are highly targeted to specific subcellular domains corresponding to sites of intense cargo function and/or release. Classic examples of highly asymmetrically distributed organelles include SVs and constitutive secretory vesicles housing membrane proteins; more subtle asymmetry is exemplified by mitochondria (42,48,64,65). In contrast, asymmetry in the distribution of mammalian DCVs is controversial (27).

To address this controversy, we used fluorescence microscopy and quadrat analysis to develop a quantitative model of DCV organization in spontaneously active hippocampal neurons and to assay putative asymmetry in DCV organization. Our results reveal that DCV organization in this system is globally stochastic, and that there is small-scale, local presynaptic enrichment. The implications of these results are discussed below.

Implications of stochastic organization

A major result of this work is that the distribution of DCVs within synapses, and in synapse-sized subdomains along shafts of axons and dendrites, follows Poisson statistics. More specifically, we find that spines and boutons average ~0.7 DCVs per site, and that in both subdomains the

distribution about the mean is very well described by Poisson statistics. DCVs in synapse-sized subdomains along axons and dendrites are distributed similarly, with one important distinction: in extrasynaptic axonal subdomains, occupancy per unit area is 1/(3.26) to 1/(2.55), or ~30–40%, of that in boutons.

There are several important implications of these results. One follows from the properties of the Poisson distribution, which describes the distribution of events when the allowed outcomes are integral, the average event rate is known, and the outcomes are independent and random (66). The first two conditions clearly hold here, and we conclude that the third also is satisfied in light of the excellent fit of our data to the Poisson distribution. Thus, DCVs localize in subcellular domains randomly. In marked contrast, organelles like SVs are targeted actively to specific subcellular domains in vivo and in vitro (67,68).

Randomness in DCV organization also implies that hippocampal neurons can meet the demands for the function of DCV cargo via organization that in part is passively dictated. The primary caveat is that active transport propels DCVs away from sites of synthesis (33).

Implications of presynaptic enrichment

A second major result of this work is that DCVs are enriched in boutons of spontaneously active hippocampal neurons. We focused on spontaneously active neurons for two reasons. First, enrichment in these is more poorly studied than in their stimulated counterparts. Second, a small body of past work suggests synaptic enrichment of mitochondria in spontaneously active neurons, and this made it plausible to test for similar enrichment of DCVs. Both of these motivational issues are discussed in more detail below under Comparison with Past Work.

One potentially biologically relevant function of synaptic enrichment is protecting boutons from depletion of DCV cargo by enhancing cargo prevalence. Evidence suggesting that this is important comes from both invertebrate and vertebrate systems. For example, boutons in *Drosophila* and cat undergo robust poststimulus depletion of DCVs (29,30). In the latter case, depletion can be temporally very long-lived, and this has been hypothesized to reflect the fact that boutons are potentially quite distant from sites of DCV synthesis/replenishment in the soma. Depletion is significantly less long-lived in *Drosophila*. Possible reasons for this difference include shorter process length in *Drosophila* and/or the fact that replenishment in *Drosophila* is made much more efficient by augmenting slow resupply from the soma with more rapid resupply from a circulating pool of axonal DCVs (16).

There are several mechanisms that could plausibly lead to presynaptic enrichment. These include binding site enrichment/preferential capture in boutons and/or a reduced average DCV transport rate in boutons relative to axon shafts. As with highway traffic, a reduction in DCV speed will tend to increase congestion, thereby enhancing DCV occupancy of boutons. Consistent with this hypothesis, bouton-associated slowing of vesicles tagged with SV markers has been observed with stimulated emission depletion microscopy, which has the superresolution required to quantify transport in bouton-sized regions (69). Such slowing could reflect a stick-and-diffuse mechanism of SV motion in boutons or diffusion within a cage (70).

Implications for synaptic organization

The results obtained here also contribute to a growing body of evidence revealing marked compositional and organizational variability at synapses (71–73) by demonstrating that DCV occupancy of synapses is stochastic, with boutons and spines typically housing from zero to three DCVs.

The biological relevance of this, and related, synaptic variability is uncertain but is the focus of both interest and speculation (31,72). In a similarly speculative spirit, we note that synaptic DCV occupancies ranging from zero to three imply marked differences in synaptic abundance of BDNF and tPA. Most notably, a substantial fraction of synapses are devoid of these key cargo proteins, and this has the potential to give rise to significant variability in synaptic responses to stimuli that induce learning and memory formation.

Implications for in vivo systems

One potential concern is that stochastic organization of DCVs is a property of cultured neurons and not of neurons in vivo. However, we feel that this is not a likely scenario for two primary reasons. First, other organelles in cultured neurons, like SVs and vesicles that transport membrane proteins, are correctly (and asymmetrically) targeted to their appropriate subcellular domains (74–76). Thus, cultured neurons appear to be a generally valid model for studying organelle organization. Second, a comprehensive review of past (more qualitative) studies of DCV organization in mammalian systems revealed considerable agreement between results obtained from in vitro and in vivo systems (10), although some disparity has been observed (9).

Comparison with past work

We close by comparing our results with results from the literature that are particularly relevant. The first of these literature results addresses DCV organization in nonmammalian and mammalian neurons and emphasizes the possibility of stimulation-induced recruitment to synapses. The

second addresses mitochondrial organization in spontaneously active neurons and focuses on statistics of organization and putative synaptic enrichment. Also relevant are dynamic data demonstrating sporadic capture of DCVs by boutons in *Drosophila* (16).

Motivated largely by the pivotal role that DCV cargo proteins play in synaptic plasticity, considerable effort has been directed at testing for physiologically relevant, stimulation-induced enrichment of DCVs at synapses (17,18). To date, the most compelling experimental evidence in support of this possibility has been obtained from nonmammalian systems. For example, DCVs are recruited into boutons of *Drosophila* motor neurons in response to electrical and chemical stimuli, and DCVs accumulate in optical tectal synapses of *Xenopus laevis* under conditions of chronic visual deprivation (77,78). More suggestive evidence has been obtained from mammalian systems. For example, DCVs in hippocampal neurons undergo modest recruitment to synaptic sites in response to relatively long-lived stimulation with glycine and 4-aminopyridine plus bicuculline (79,80).

Here we have focused instead on testing for putative synaptic enrichment of DCVs in spontaneously active neurons, and our data provide, to our knowledge, some of the first compelling evidence in support of this possibility by revealing presynaptic enrichment relative to nearby regions of shafts in hippocampal neurons from rat. Somewhat related, less rigorous, past studies of enrichment in hippocampal neurons from mice, which did not include quantitative comparison between synapses and shafts, have produced contradictory conclusions. In one case, the conclusion was an absence of presynaptic enrichment, and in another case the presence of presynaptic enrichment (8,28). Our data also refute the enrichment hypothesis for the case of postsynaptic sites in hippocampal neurons.

Motivated by an interest in addressing hypotheses similar to those surrounding DCVs (81,82), effort also has been directed at statistical analysis of mitochondrial organization and at assaying for mitochondrial enrichment at synapses in neurons that are spontaneously active. Upon comparison of results, we find some intriguing parallels. For example, our mean axonal $VMR = 0.94$ is quite similar to the mean axonal $VMR = 0.73$ reported for mitochondria in chicken dorsal root ganglion neurons (48). Moreover, one of our presynaptic enrichment values, $ER = 255\%$, is very similar to the $ER = 252\%$ reported for mitochondria in spontaneously active cortical neurons (42). In contrast, our data reveal no evidence for postsynaptic enrichment of DCVs, whereas ~50% postsynaptic enrichment has been reported for mitochondria in cortical neurons (42).

CONCLUSIONS

We have conducted detailed statistical analysis and modeling of DCV organization in spontaneously active hippocampal neurons that provide insight into mechanisms of DCV cargo action. Our analysis reveals that DCV organization along processes and within synapses of spontaneously active hippocampal neurons follows Poisson statistics, with mean Poisson occupancy in boutons exceeding occupancy in nearby regions of shafts by approximately threefold. One important implication of these results is that DCVs in spontaneously active hippocampal neurons are randomly organized. Random organization of organelles is relatively unusual but is consistent with the wide-ranging spatial character of DCV cargo function. Our analysis also establishes the validity of the presynaptic enrichment hypothesis and thereby suggests a mechanism of protecting presynaptic sites from depletion of DCV cargo. Future work directed at identifying, and quantifying the distribution of, putative DCV binding proteins in mammalian neurons will help to determine the extent to which stochastically dictated organization of DCVs has its origin in processes such as random deposition and/or binding to randomly distributed sites.

AUTHOR CONTRIBUTIONS

B.J.R. performed experiments and contributed to the analysis; B.S. performed experiments; M.A.S. supervised and performed experiments, and contributed to the writing of the article; and B.A.S. designed the study, supervised and performed experiments, contributed to the analysis, and played a key role in writing the article.

ACKNOWLEDGMENTS

We thank Dr. Gary Banker and Barbara Smoody of Oregon Health and Sciences University for advice and for extensive support with the culture of hippocampal neurons, and Dr. James Abney for a critical reading of this article.

This work was supported by National Institutes of Health grant No. 2 R15 GM061539-02 (to B.A.S.) and Natural Sciences and Engineering Research Council grant No. 327100-2011 (to M.A.S.).

REFERENCES

1. Perlson, E., S. Maday, …, E. L. Holzbaur. 2010. Retrograde axonal transport: pathways to cell death? *Trends Neurosci.* 33:335–344.
2. Hinckelmann, M. V., D. Zala, and F. Saudou. 2013. Releasing the brake: restoring fast axonal transport in neurodegenerative disorders. *Trends Cell Biol.* 23:634–643.
3. Maday, S., A. E. Twelvetrees, …, E. L. Holzbaur. 2014. Axonal transport: cargo-specific mechanisms of motility and regulation. *Neuron.* 84:292–309.
4. Maeder, C. I., K. Shen, and C. C. Hoogenraad. 2014. Axon and dendritic trafficking. *Curr. Opin. Neurobiol.* 27:165–170.
5. Kononenko, N. L., and V. Haucke. 2015. Molecular mechanisms of presynaptic membrane retrieval and synaptic vesicle reformation. *Neuron.* 85:484–496.
6. Kevenaar, J. T., and C. C. Hoogenraad. 2015. The axonal cytoskeleton: from organization to function. *Front. Mol. Neurosci.* 8:44.
7. Park, H., and M. M. Poo. 2013. Neurotrophin regulation of neural circuit development and function. *Nat. Rev. Neurosci.* 14:7–23.
8. Andreska, T., S. Aufmkolk, …, R. Blum. 2014. High abundance of BDNF within glutamatergic presynapses of cultured hippocampal neurons. *Front. Cell. Neurosci.* 8:107.

9. Dieni, S., T. Matsumoto, …, Y. A. Barde. 2012. BDNF and its pro-peptide are stored in presynaptic dense core vesicles in brain neurons. *J. Cell Biol.* 196:775–788.
10. Edelmann, E., V. Lessmann, and T. Brigadski. 2014. Pre- and postsynaptic twists in BDNF secretion and action in synaptic plasticity. *Neuropharmacology.* 76:610–627.
11. Lochner, J. E., L. S. Honigman, …, B. A. Scalettar. 2006. Activity-dependent release of tissue plasminogen activator from the dendritic spines of hippocampal neurons revealed by live-cell imaging. *J. Neurobiol.* 66:564–577.
12. Scalettar, B. A., C. Jacobs, …, J. E. Lochner. 2012. Hindered submicron mobility and long-term storage of presynaptic dense-core granules revealed by single-particle tracking. *Dev. Neurobiol.* 72:1181–1195.
13. Goodwin, P. R., J. M. Sasaki, and P. Juo. 2012. Cyclin-dependent kinase 5 regulates the polarized trafficking of neuropeptide-containing dense-core vesicles in *Caenorhabditis elegans* motor neurons. *J. Neurosci.* 32:8158–8172.
14. Hill, S. E., M. Parmar, …, M. M. Rolls. 2012. Development of dendrite polarity in *Drosophila* neurons. *Neural Dev.* 7:34.
15. Rolls, M. M. 2011. Neuronal polarity in *Drosophila*: sorting out axons and dendrites. *Dev. Neurobiol.* 71:419–429.
16. Wong, M. Y., C. Zhou, …, E. S. Levitan. 2012. Neuropeptide delivery to synapses by long-range vesicle circulation and sporadic capture. *Cell.* 148:1029–1038.
17. Baranes, D., D. Lederfein, …, E. R. Kandel. 1998. Tissue plasminogen activator contributes to the late phase of LTP and to synaptic growth in the hippocampal mossy fiber pathway. *Neuron.* 21:813–825.
18. Korte, M., P. Carroll, …, T. Bonhoeffer. 1995. Hippocampal long-term potentiation is impaired in mice lacking brain-derived neurotrophic factor. *Proc. Natl. Acad. Sci. USA.* 92:8856–8860.
19. Lochner, J. E., E. Spangler, …, B. A. Scalettar. 2008. Efficient copackaging and cotransport yields postsynaptic colocalization of neuromodulators associated with synaptic plasticity. *Dev. Neurobiol.* 68:1243–1256.
20. van den Pol, A. N. 2012. Neuropeptide transmission in brain circuits. *Neuron.* 76:98–115.
21. Blankenship, A. G., and M. B. Feller. 2010. Mechanisms underlying spontaneous patterned activity in developing neural circuits. *Nat. Rev. Neurosci.* 11:18–29.
22. Mazzoni, A., F. D. Broccard, …, V. Torre. 2007. On the dynamics of the spontaneous activity in neuronal networks. *PLoS One.* 2:e439.
23. Kilb, W., S. Kirischuk, and H. J. Luhmann. 2011. Electrical activity patterns and the functional maturation of the neocortex. *Eur. J. Neurosci.* 34:1677–1686.
24. Luczak, A., and J. N. MacLean. 2012. Default activity patterns at the neocortical microcircuit level. *Front. Integr. Neurosci.* 6:30.
25. Raichle, M. E. 2006. Neuroscience. The brain's dark energy. *Science.* 314:1249–1250.
26. Kuczewski, N., C. Porcher, …, J. L. Gaiarsa. 2008. Backpropagating action potentials trigger dendritic release of BDNF during spontaneous network activity. *J. Neurosci.* 28:7013–7023.
27. Lessmann, V., and T. Brigadski. 2009. Mechanisms, locations, and kinetics of synaptic BDNF secretion: an update. *Neurosci. Res.* 65:11–22.
28. van de Bospoort, R., M. Farina, …, R. F. Toonen. 2012. Munc13 controls the location and efficiency of dense-core vesicle release in neurons. *J. Cell Biol.* 199:883–891.
29. Shakiryanova, D., A. Tully, …, E. S. Levitan. 2005. Activity-dependent liberation of synaptic neuropeptide vesicles. *Nat. Neurosci.* 8:173–178.
30. Weldon, P., M. Bachoo, and C. Polosa. 1990. Depletion by preganglionic stimulation and post-stimulus recovery of large dense core vesicles in synaptic boutons of the cat superior cervical ganglion. *Brain Res.* 516:341–344.
31. Ribrault, C., K. Sekimoto, and A. Triller. 2011. From the stochasticity of molecular processes to the variability of synaptic transmission. *Nat. Rev. Neurosci.* 12:375–387.
32. Rat hippocampal neurons in low-density culture. *In* Culturing Nerve Cells. K. Goslin and G. Banker, editors. MIT Press, Cambridge, MA, pp. 339–370.
33. Lochner, J. E., M. Kingma, …, B. A. Scalettar. 1998. Real-time imaging of the axonal transport of granules containing a tissue plasminogen activator/green fluorescent protein hybrid. *Mol. Biol. Cell.* 9:2463–2476.
34. Ohki, E. C., M. L. Tilkins, …, P. J. Price. 2001. Improving the transfection efficiency of post-mitotic neurons. *J. Neurosci. Methods.* 112:95–99.
35. Ho, D. Y. 1994. Amplicon-based herpes simplex virus vectors. *Methods Cell Biol.* 43:191–210.
36. Binder, L. I., A. Frankfurter, and L. I. Rebhun. 1985. The distribution of tau in the mammalian central nervous system. *J. Cell Biol.* 101:1371–1378.
37. Bernhardt, R., and A. Matus. 1984. Light and electron microscopic studies of the distribution of microtubule-associated protein 2 in rat brain: a difference between dendritic and axonal cytoskeletons. *J. Comp. Neurol.* 226:203–221.
38. Kolarow, R., T. Brigadski, and V. Lessmann. 2007. Postsynaptic secretion of BDNF and NT-3 from hippocampal neurons depends on calcium calmodulin kinase II signaling and proceeds via delayed fusion pore opening. *J. Neurosci.* 27:10350–10364.
39. Matsuda, N., H. Lu, …, M. M. Poo. 2009. Differential activity-dependent secretion of brain-derived neurotrophic factor from axon and dendrite. *J. Neurosci.* 29:14185–14198.
40. Swanwick, C. C., M. B. Harrison, and J. Kapur. 2004. Synaptic and extrasynaptic localization of brain-derived neurotrophic factor and the tyrosine kinase B receptor in cultured hippocampal neurons. *J. Comp. Neurol.* 478:405–417.
41. Scalettar, B. A., J. R. Swedlow, …, D. A. Agard. 1996. Dispersion, aberration and deconvolution in multi-wavelength fluorescence images. *J. Microsc.* 182:50–60.
42. Chang, D. T., A. S. Honick, and I. J. Reynolds. 2006. Mitochondrial trafficking to synapses in cultured primary cortical neurons. *J. Neurosci.* 26:7035–7045.
43. Burke, N. V., W. Han, …, E. S. Levitan. 1997. Neuronal peptide release is limited by secretory granule mobility. *Neuron.* 19:1095–1102.
44. Silverman, M. A., S. Johnson, …, B. A. Scalettar. 2005. Mechanisms of transport and exocytosis of dense-core granules containing tissue plasminogen activator in developing hippocampal neurons. *J. Neurosci.* 25:3095–3106.
45. Abney, J. R., C. D. Meliza, …, B. A. Scalettar. 1999. Real-time imaging of the dynamics of secretory granules in growth cones. *Biophys. J.* 77:2887–2895.
46. Saxton, M. J., and K. Jacobson. 1997. Single-particle tracking: applications to membrane dynamics. *Annu. Rev. Biophys. Biomol. Struct.* 26:373–399.
47. Shaw, P. J. 2006. Comparison of widefield/deconvolution and confocal microscopy for three-dimensional imaging. *In* Handbook of Biological Confocal Microscopy. J. B. Pawley, editor. Springer Science + Business Media, New York, pp. 453–467.
48. Miller, K. E., and M. P. Sheetz. 2004. Axonal mitochondrial transport and potential are correlated. *J. Cell Sci.* 117:2791–2804.
49. Shepherd, G. M., and K. M. Harris. 1998. Three-dimensional structure and composition of CA3→CA1 axons in rat hippocampal slices: implications for presynaptic connectivity and compartmentalization. *J. Neurosci.* 18:8300–8310.
50. McGrew, J. C., A. J. Lembo, and C. B. Monroe. 2014. An Introduction to Statistical Problem Solving in Geography. Waveland Press, Long Grove, IL.
51. de Smith, M. J., M. F. Goodchild, and P. A. Longley. 2015. Geospatial Analysis: A Comprehensive Guide to Principles, Techniques, and Software Tools. Winchelsea Press, Leicester, UK.
52. O'Sullivan, D. U., and J. David. 2010. Geographic Information Analysis. John Wiley, Hoboken, NJ.

53. Svetlitsky, V. A. 2003. Statistical Dynamics and Reliability Theory for Mechanical Structures. Springer, Berlin, Germany.

54. Moran, P. A. 1950. Notes on continuous stochastic phenomena. *Biometrika.* 37:17–23.

55. Sawada, M. 1999. ROOKCASE: an Excel 97/2000 visual basic (VB) add-in for exploring global and local spatial autocorrelation. *Bull. Ecol. Soc. Am.* 80:231–234.

56. Xia, J., S. Cai, …, S. Nie. 2015. Spatial, temporal, and spatiotemporal analysis of malaria in Hubei Province, China from 2004–2011. *Malar. J.* 14:145.

57. Moore, D. S. M. G. P. 2003. Introduction to the Practice of Statistics. W. H. Freeman, New York.

58. Lee, J., and D. W. S. Wong. 2001. Statistical Analysis with ArcView GIS. John Wiley, New York.

59. Haubensak, W., F. Narz, …, V. Lessmann. 1998. BDNF-GFP containing secretory granules are localized in the vicinity of synaptic junctions of cultured cortical neurons. *J. Cell Sci.* 111:1483–1493.

60. Hartmann, M., R. Heumann, and V. Lessmann. 2001. Synaptic secretion of BDNF after high-frequency stimulation of glutamatergic synapses. *EMBO J.* 20:5887–5897.

61. Steyer, J. A., H. Horstmann, and W. Almers. 1997. Transport, docking and exocytosis of single secretory granules in live chromaffin cells. *Nature.* 388:474–478.

62. Xia, X., V. Lessmann, and T. F. Martin. 2009. Imaging of evoked dense-core-vesicle exocytosis in hippocampal neurons reveals long latencies and kiss-and-run fusion events. *J. Cell Sci.* 122:75–82.

63. Lee, Y.-H. 2015. Spatial and temporal analysis of glutamate receptor localisation at the *Drosophila* neuromuscular junction. Dissertation. Humboldt-Universität zu Berlin, Lebenswissenschaftliche Fakultät, Berlin, Germany.

64. Lippincott-Schwartz, J., T. H. Roberts, and K. Hirschberg. 2000. Secretory protein trafficking and organelle dynamics in living cells. *Annu. Rev. Cell Dev. Biol.* 16:557–589.

65. Sudhof, T. C. 2004. The synaptic vesicle cycle. *Annu. Rev. Neurosci.* 27:509–547.

66. Taylor, J. R. 1997. An Introduction to Error Analysis. University Science Books, South Orange, NJ.

67. Ahmari, S. E., J. Buchanan, and S. J. Smith. 2000. Assembly of presynaptic active zones from cytoplasmic transport packets. *Nat. Neurosci.* 3:445–451.

68. Wu, Y. E., L. Huo, …, K. Shen. 2013. The balance between capture and dissociation of presynaptic proteins controls the spatial distribution of synapses. *Neuron.* 78:994–1011.

69. Westphal, V., S. O. Rizzoli, …, S. W. Hell. 2008. Video-rate far-field optical nanoscopy dissects synaptic vesicle movement. *Science.* 320:246–249.

70. Yeung, C., M. Shtrahman, and X. L. Wu. 2007. Stick-and-diffuse and caged diffusion: a comparison of two models of synaptic vesicle dynamics. *Biophys. J.* 92:2271–2280.

71. Harris, K. M., and P. Sultan. 1995. Variation in the number, location and size of synaptic vesicles provides an anatomical basis for the nonuniform probability of release at hippocampal CA1 synapses. *Neuropharmacology.* 34:1387–1395.

72. Parker, D. 2015. Synaptic variability introduces state-dependent modulation of excitatory spinal cord synapses. *Neural Plast.* 2015:512156.

73. Racca, C., F. A. Stephenson, …, P. Somogyi. 2000. NMDA receptor content of synapses in stratum radiatum of the hippocampal CA1 area. *J. Neurosci.* 20:2512–2522.

74. Craig, A. M., C. D. Blackstone, …, G. Banker. 1994. Selective clustering of glutamate and γ-aminobutyric acid receptors opposite terminals releasing the corresponding neurotransmitters. *Proc. Natl. Acad. Sci. USA.* 91:12373–12377.

75. Silverman, M. A., S. Kaech, …, G. Banker. 2001. Sorting and directed transport of membrane proteins during development of hippocampal neurons in culture. *Proc. Natl. Acad. Sci. USA.* 98:7051–7057.

76. Zhai, R. G., H. Vardinon-Friedman, …, C. C. Garner. 2001. Assembling the presynaptic active zone: a characterization of an active one precursor vesicle. *Neuron.* 29:131–143.

77. Li, J., and H. T. Cline. 2010. Visual deprivation increases accumulation of dense core vesicles in developing optic tectal synapses in *Xenopus laevis*. *J. Comp. Neurol.* 518:2365–2381.

78. Shakiryanova, D., A. Tully, and E. S. Levitan. 2006. Activity-dependent synaptic capture of transiting peptidergic vesicles. *Nat. Neurosci.* 9:896–900.

79. Dean, C., H. Liu, …, E. R. Chapman. 2012. Distinct subsets of Syt-IV/BDNF vesicles are sorted to axons versus dendrites and recruited to synapses by activity. *J. Neurosci.* 32:5398–5413.

80. Petoukhov, E., S. Fernando, …, S. X. Bamji. 2013. Activity-dependent secretion of progranulin from synapses. *J. Cell Sci.* 126:5412–5421.

81. Bulgari, D., C. Zhou, …, E. S. Levitan. 2014. Vesicle capture, not delivery, scales up neuropeptide storage in neuroendocrine terminals. *Proc. Natl. Acad. Sci. USA.* 111:3597–3601.

82. Nurrish, S. 2014. Dense core vesicle release: controlling the where as well as the when. *Genetics.* 196:601–604.